ELSEVIER

Journal of Alloys and Compounds 317–318 (2001) 503–512

Journal of ALLOYS AND COMPOUNDS

www.elsevier.com/locate/jallcom

Effect of Cu and Zn on the melting and transformation temperatures of Pr and Gd

A. Saccone*, A.M. Cardinale, S. Delfino, G. Cacciamani, R. Ferro

Dipartimento di Chimica e Chimica Industriale, Università di Genova, Via Dodecaneso 31, I-16146 Genova, Italy

Abstract

Phase equilibria in the R-rich regions of the R-Cu and R-Zn binary systems (R=Pr and Gd) have been investigated by differential thermal analysis, X-ray powder diffractometry, metallographic analysis and quantitative electron probe microanalysis. In these regions, the lowering (ΔT) of the melting and transformation temperatures of the rare earth metals by addition of copper and zinc resulted in eutectic and catatectic or eutectoidal type reactions. The ΔT observed in these systems are discussed and compared with those reported in the literature for the binary systems of Pr and Gd with Mg and with the elements from the 9th to the 14th group of the Periodic Table. In order to complete this systematics, a few Pr-rich Pr–Cd alloys have also been prepared and analysed.

Keywords: Phase diagrams; Rare earth alloys; Copper alloys; Zinc alloys

1. Introduction

The R-Cu and R-Zn (R=rare earth metal) binary alloy systems are characterized by the existence of several intermetallic compounds often showing complex and high temperature melting equilibria.

A number of phase diagrams of the R-Cu and R-Zn systems with the trivalent rare earths have been partially or completely investigated. They are reported in compilations such as [1,2], even though data relevant to the R-rich part of these diagrams are generally lacking and in some case conflicting.

The goal of this study was to investigate the effect of Cu and Zn additions on the melting and transition temperatures (from the high temperature cubic, bcc, to the low temperature hexagonal, dhcp and hcp, structures) of the two typical rare earth metals, Pr and Gd, representing the behaviour of the light and heavy lanthanides, respectively.

2. Literature data

2.1. Pr–Cu system

The Pr–Cu system was investigated by Canneri [3]; more recently Subramanian and Laughlin [4] assessed the system mainly considering the data by Canneri, although the Pr used in the experiments by Canneri [3] was quite impure. However, the temperatures of a few invariant equilibria were modified on the basis of the interpolation of data obtained for other Cu-lanthanide systems, considering also the crystallographic investigation by Dwight [5] who identified the $PrCu_5$ phase.

In the assessed Pr–Cu system, five intermetallic phases are reported to exist, namely: PrCu (orthorhombic, oP8-FeB type, peritectic formation at 563°C), $PrCu_2$ (orthorhombic, oI12-$CeCu_2$ type, m.p. 841°C), $PrCu_4$ (orthorhombic, oP20-$CeCu_4$ type, per. form. 824°C), $PrCu_5$ (hexagonal, hP6-$CaCu_5$ type, per. form. 837°C) and $PrCu_6$ (orthorhombic, oP28-$CeCu_6$ type, m.p. 962°C). Three eutectic equilibria are reported between (αPr) and PrCu (at 472°C and 32 at% Cu), $PrCu_2$ and $PrCu_4$ (at 770°C and ≈73at% Cu) and $PrCu_6$ and (Cu) (at 870°C and ≈92.5 at% Cu). All the compounds are indicated as line compounds. The terminal solid solubilities and the solid state equilibrium involving praseodymium were not studied.

2.2. Gd–Cu system

The Gd–Cu system was investigated by a number of researchers. Copeland and Kato [6] studied the Gd-rich region of the system. Subsequently Carnasciali et al. [7]

*Corresponding author. Tel.: +39-010-353-6154.
E-mail address: saccone@chimica.unige.it (A. Saccone).

0925-8388/01/$ – see front matter
PII: S0925-8388(00)01378-5

and Cheng and Zeng [8] determined independently the Gd–Cu system, but the two reports show discrepancies on the existence and on the mechanism of formation of some phases. An assessed version of the system was reported by Subramanian et al. [9], mainly based on the diagram proposed by Carnasciali et al. [7], since it follows closely the systematics of Cu with the heavy lanthanides, with adjustments in the elemental melting points in accordance with the accepted values [1].

The assessed version of the Gd–Cu system shows seven intermetallic compounds: GdCu (cubic, cP2-CsCl type, m.p 830°C), $GdCu_2$ (orthorhombic, oI12-$CeCu_2$ type, m.p. 860°C), Gd_2Cu_7 (unknown structure, detected on the basis of thermal effects only, peritectic fomation at 870°C followed by catatectic decomposition at 825°C giving rise to Gd_2Cu_9 and liquidus), Gd_2Cu_9 (structure based on a tetragonal cell, m.p. 930°C), $GdCu_5$ (high temperature form, hexagonal, hP6-$CaCu_5$ type; room temperature form, cubic, cF24-$AuBe_5$ type, per. form. 925°C, allotropic transformation at 870°C), $GdCu_6$ (orthorhombic, oP28-$CeCu_6$ type, per. form. 865°C) and $GdCu_7$ (structure based on a hexagonal cell, peritectic or peritectoidal formation very near to the Cu-rich eutectic followed by eutectoidal decomposition to $GdCu_6$ and (Cu) at about 700°C).

Four eutectic equilibria are reported between (βGd) and GdCu (at 675°C and 30 at% Cu), GdCu and $GdCu_2$ (at 770°C and 56 at% Cu), $GdCu_2$ and Gd_2Cu_9 (at 820°C and 71 at% Cu) and $GdCu_6$ and (Cu) (at 860°C and 90.5 at% Cu). All the compounds are indicated as line compounds with the exception of $GdCu_5$ for which a range of about 1.3 at% is suggested. According to Carnasciali et al. [7], (βGd) undergoes a eutectoidal decomposition to (αGd) and GdCu at 630°C and 10.5 at% Cu. The solid solubilities of Cu in αGd and βGd were tentatively estimated, on the basis of DTA results, to be ≈2 at% and ≈15 at%, respectively. There is no evidence of any terminal solid solubility of Gd in Cu.

2.3. Pr–Zn system

The Pr–Zn system has been studied by Mason and Chiotti [10]. The crystal structure of the intermetallic phases are also reported by Villars et al. [11]. Seven intermetallic compounds occur: PrZn (L.T. form, tetragonal, tP2-HgMn type, H.T. form, cubic, cP2-CsCl type, m.p. 882°C), $PrZn_2$ (L.T. form, orthorhombic, oI12-$CeCu_2$ type, H.T. form, unknown structure, m.p. 898°C), $PrZn_3$ (orthorhombic, oP16-YZn_3 type, per. form. 833°C), Pr_3Zn_{11} (orthorhombic, oI28-$Al_{11}La_3$, per. form. 855°C), $Pr_{13}Zn_{58}$ (hexagonal, hP142-$Gd_{13}Zn_{58}$, per. form. 891°C), Pr_3Zn_{22} (tetragonal, tI100-Pu_3Zn_{22} type, per. form. 956°C), Pr_2Zn_{17} (L.T. form hexagonal, hP38-$Ni_{17}Th_2$ type, H.T. form, rhombohedral, hR57-Th_2Zn_{17} type, m.p. 978°C) and $PrZn_{11}$ (tetragonal, tI48-$BaCd_{11}$ type, per. form. 743°C). Three eutectic equilibria have been reported to occur: at 576°C and 22.5 at% Zn (between (βPr) and PrZn), at 833°C and 57.9 at% Zn (between PrZn and $\beta PrZn_2$), at 830°C and 73.9 at% Zn (between $\beta PrZn_2$ and $PrZn_3$). A eutectoidal reaction occurs in the Pr-rich end, at 558°C and 10.6 at% Zn (decomposition in the solid state of the (βPr) in (αPr) and PrZn). The maximum solid solubility of Zn in βPr is 11 at% Zn (at the eutectic temperature); the solubility of Zn in αPr and that of Pr in Zn are practically negligible.

2.4. Gd–Zn system

No equilibrium diagram is available for the Gd–Zn system. A schematic drawing is reported in Massalski et al. [1] on the basis both of the existence of the known intermediate phases and of the melting and eutectic temperatures of the Zn-lanthanide systems showing a systematic variation across the lanthanide series. In addition to the phases showing the same stoichiometries (with the exception of RZn_{11}) reported in the Pr–Zn system (and in the schematic Gd–Zn diagram presented in [1]), other intermetallic compounds are known: Gd_6Zn_{23} (cubic, cF116-Th_6Mn_{23}), $GdZn_5$ (hexagonal, hP6-$CaCu_5$), $GdZn_{12}$ (tetragonal, tI26-$ThMn_{12}$) (see Refs. [1,11]).

3. Experimental techniques

The purity of the elements was 99.999 mass% in the case of Cu and Zn and 99.9 mass% for Pr and Gd. All the elements were supplied by Koch Chemicals Ltd., Hertford, UK. Major impurity elements in praseodymium and gadolinium, detected by spectrographic method, were (all the values in mass%): Y (<0.05), La (<0.05), Sm (0.06), Pr (<0.05), Si (0.01), Fe (<0.01), Mg (<0.01), Ca (<0.01), Al (<0.01), Ni(<0.01). Differential thermal analysis carried out on the Pr and Gd metals gave the following results: Pr: m.p. 929°C (instead of the accepted values of 931°C, from [12]), $\alpha \rightleftarrows \beta$ transformation temperature 798°C (instead of 795°C), Gd: m.p 1315°C (instead of 1313°C), $\alpha \rightleftarrows \beta$ transformation temperature 1239°C (instead of 1235°C).

Differential thermal analysis and X-ray diffraction were also performed on pure copper and zinc, giving the following data: m.p Cu. 1082°C (instead of 1085°C), m.p Zn 419°C (literature: 419°C); lattice parameter Cu $a=$ 0.3612 nm (in comparison with the literature value $a=$ 0.3614 nm [1]), Zn $a=0.2665$ nm, $c=0.4947$ nm (literature values: $a=0.2664$ nm, $c=0.4947$ nm).

Samples were prepared by weighing small pieces of the pure elements in small tantalum crucibles. The crucibles, closed by electric arc welding under argon atmosphere, were induction-heated up to the melting point in a vacuum tube furnace which could also be filled with an inert atmosphere. Homogenization was obtained by repeated

shaking of the crucibles. No side reactions at high temperature with the crucibles have been found.

After melting, different heat treatments were performed, according to the kind of analysis or measurement planned for each sample.

Differential thermal analysis, X-ray powder diffractometry, metallographic analysis and quantitative electron probe microanalysis were used to characterize the samples.

- Differential thermal analysis with heating and cooling rates between 2 and 10 K min^{-1}, using a model 404S Netzsch apparatus (Selb, Germany). In the temperature range considered, the temperature accuracy was estimated to be within ±0.5% of the measured value. The thermocouples were calibrated by using, as calibration materials, high purity elements such as Al, Ag, Au, whose melting points fall in the temperature range suitable for the investigated samples. The melting points were obtained from the DTA curves using the extrapolated onset temperatures, given by the intersection with the extrapolated baseline of the tangent drawn at the point of greatest slope on the leading edge of the peak.
- Metallographic analysis by using light optical microscopy and scanning electron microscopy; the samples were dry-polished and in some cases etched with dilute HNO_3 alchoholic solution (0.5%). Microprobe analyses based on energy-dispersive X-ray spectroscopy were also performed to check the overall composition and to obtain the compositions of the co-existing phases.
- X-ray analysis by using the Debye–Scherrer method on powder samples with Cu–K_α and/or Fe–K_α filtered radiations.

4. Results

The results obtained in the investigation of the R-rich regions (up to 50 at% M, M=Cu and Zn) of the Pr–Cu, Gd–Cu, Pr–Zn and Gd–Zn systems are shown in the following. The crystal structure analysis and the lattice parameters data both from this work and from the literature are collected in Tables 1 and 2.

The proposed Pr–Cu and Gd–Cu phase diagrams from 0 to 50 at% Cu are shown in Figs. 1 and 2; those of the Pr–Zn and Gd–Zn systems (up to 50 at% Zn) are reported in Figs. 3 and 4.

4.1. Pr–Cu system

The addition of copper lowers both the melting temperature and the transformation temperature of praseodymium to a eutectic reaction at 470°C and 30 at% Cu (in very good agreement with the literature data) and to a catatectic reaction at 780°C and ≈2 at% Cu, respectively. Evidence for the catatectic reaction was observed in the thermal analysis and metallographic studies. This is also in agreement with the Ce–Cu system in which there is experimental evidence of a catatectic reaction taking place at high temperature in the Ce-rich end of the diagram [2,17]. The maximum solubility of Cu in βPr, at the 780°C catatectic temperature, is lower than 2 at% Cu; the maximum solubility of Cu in αPr is very small, less than 0.5 at% Cu.

The typical appearance of an alloy showing catatectic reaction is reported in Fig. 5. The structure of the 470°C and 30 at% Cu eutectic can be seen in Fig. 6. The general characteristics of the catatectic reaction and the metallog-

Table 1
Crystallographic data of the intermetallic phases of the Pr-rich region of the Pr–Cu system and of the Gd-rich region of the Gd–Cu system

Phase	Structure type	Nominal composition at% Cu	Lattice parameters (nm)	Comments	Ref.
αPr	hP4-αLa	0	$a=0.36721$ $c=1.18326$	at 24°C	[12]
βPr	cI2-W	0	$a=0.413$	at 821°C	[12]
PrCu	oP8-FeB	50	$a=0.724(14)$ $b=0.433(8)$ $c=0.630(12)$		[13]
			$a=0.7242$ $b=0.4336$ $c=0.6307$		This work
αGd	hP2-Mg	0	$a=0.36336$ $c=0.57810$	at 24°C	[12]
βGd	cI2-W	0			[12]
GdCu	cP2-CsCl	50	$a=0.35020(4)$ $a=0.3503$	ann. 500°C	[14] This work

Table 2
Crystallographic data of the intermetallic phases of the Pr-rich region of the Pr–Zn system and of the Gd-rich region of the Gd–Zn system

Phase	Structure type	Nominal composition at% Zn	Lattice parameters (nm)	Comments	Ref.
αPr	hP4-αLa	0	$a=0.36721$ $c=1.18326$	at 24°C	[12]
βPr	cI2-W	0	$a=0.413$	at 821°C	[12]
PrZn H.T. form	cP2-CsCl	50	$a=0.3678$ $a=0.3679$	$T>46$ K R.T	[15] This work
L.T. form	tP2-HgMn		$a=0.3652$ $c=0.3695$	$T<46$ K	[15]
αGd	hP2-Mg	0	$a=0.36336$ $c=0.57810$	at 24°C	[12]
βGd	cI2-W	0			[12]
GdZn	cP2-CsCl	50	$a=0.3618$ $a=0.3611$		[16] This work

raphic appearances associated with this invariant equilibrium have been extensively reported by Ferro et al. [18].

The most Pr-rich phase is the equiatomic PrCu. It forms through the following peritectic reaction at 540°C (slightly lower than the value from [3]):

$$L(\approx 34.5 \text{ at\% Cu}) + PrCu_2 \rightleftarrows PrCu$$

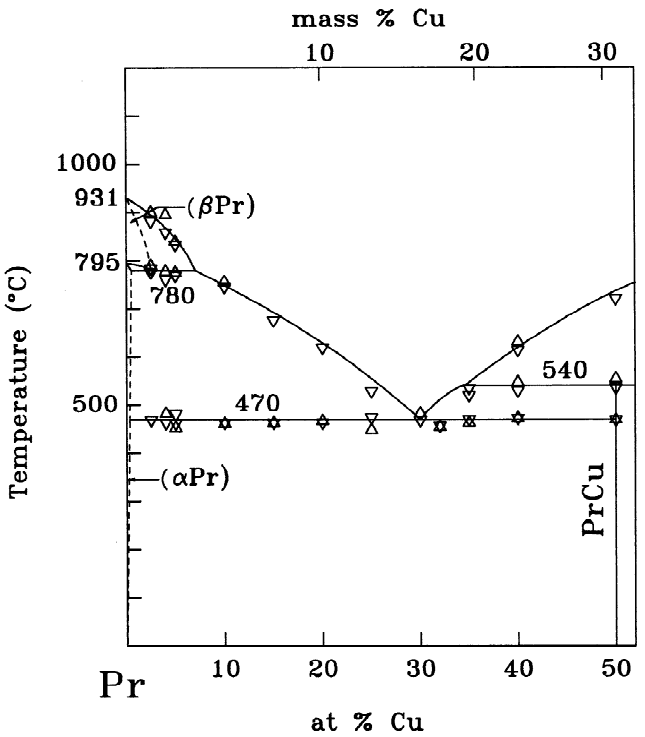

Fig. 1. Pr–Cu phase diagram (0–50 at% Cu composition range) as obtained from the experimental data (△ value on heating, ▽ value on cooling).

It is orthorhombic, oP8-FeB type; the lattice parameters reported in Table 1 are in good agreement with those of the literature [13].

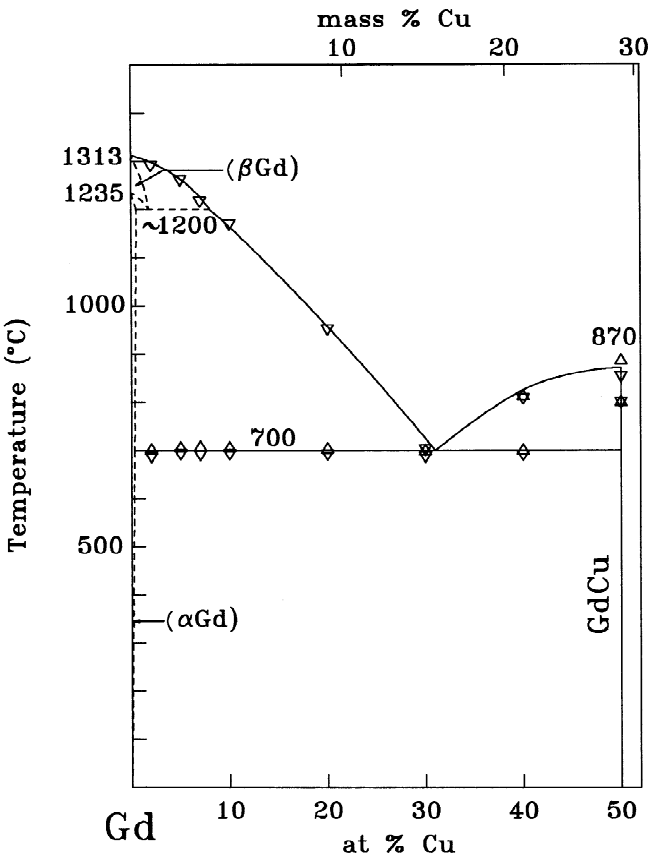

Fig. 2. Gd–Cu phase diagram (0–50 at% Cu composition range) as obtained from the experimental data (△ value on heating, ▽ value on cooling).

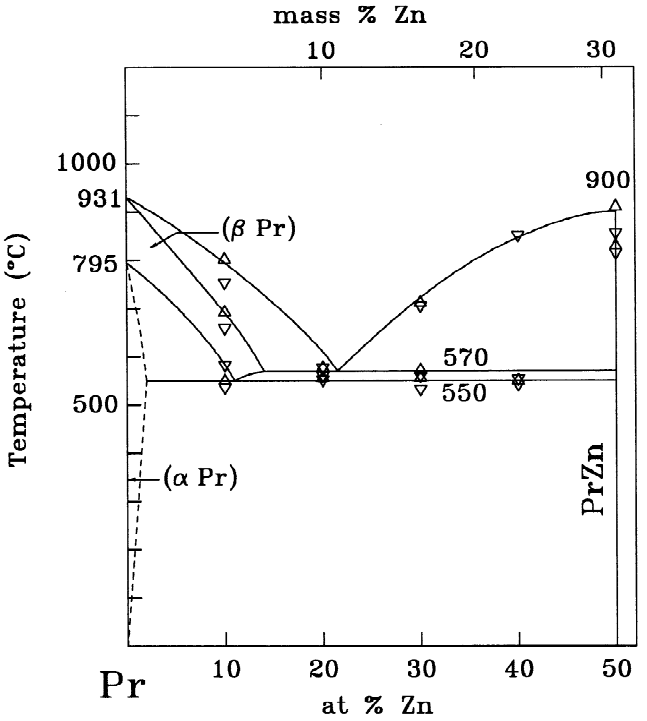

Fig. 3. Pr–Zn phase diagram (0–50 at% Zn composition range) [10]. Experimental data obtained in this work are superimposed (△ value on heating, ▽ value on cooling).

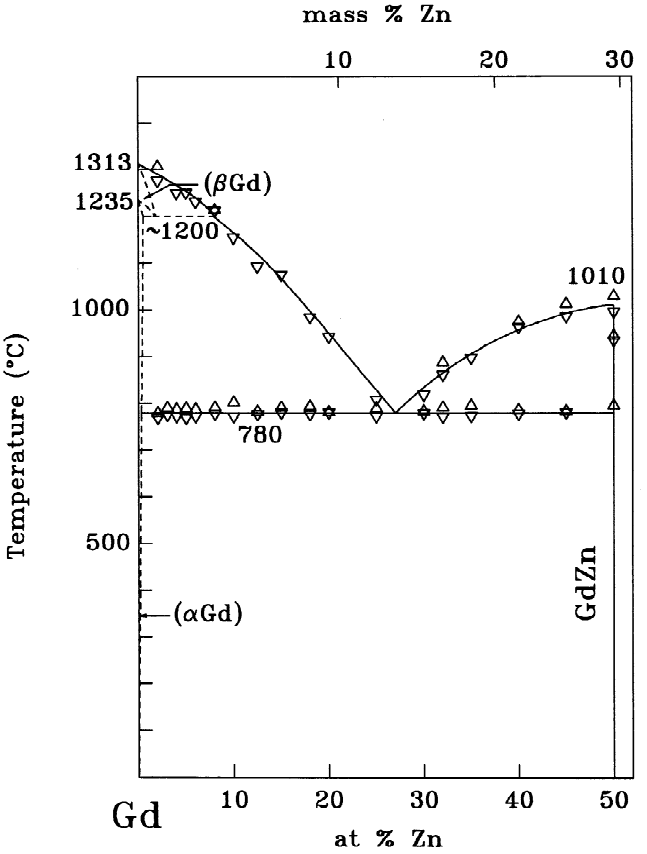

Fig. 4. Gd–Zn phase diagram (0–50 at% Zn composition range) as obtained from the experimental data (△ value on heating, ▽ value on cooling).

4.2. Gd–Cu system

Starting from pure Gd, the liquidus line decreases to a eutectic point, whose coordinates are 700°C and 31 at% Cu. The phases involved in this eutectic reaction are (αGd) and GdCu. The eutectic temperature is in fair agreement with the one reported by Carnasciali et al. [7] (675°C), but in excellent agreement with the one suggested by Copeland and Kato (700°C) in a previous report [6].

On the basis of the micrographic appearance, the following catatectic equilibrium is proposed in the Gd-rich region:

$$(\beta Gd) \rightleftarrows (\alpha Gd) + Liq$$

whose suggested coordinates are: (βGd): <2 at% Cu; (αGd): <0.5 at% Cu; Liq ≈8 at% Cu at $T \approx 1200$°C. Because of the very small heat involved in this type of reaction, no information on the catatectic temperature have been obtained by differential thermal analysis.

The results obtained in this work about the effect of Cu on the $\alpha \rightleftarrows \beta$ transformation of Gd are in contrast with those reported in the literature by Carnasciali et al. [7], who reported a maximum solid solubility of about 15 at% Cu in βGd at the Gd-rich eutectic temperature and the eutectoidal decomposition of the (βGd) in (αGd) e GdCu. This behaviour seemed quite unusual (as also pointed out by Subramanian and Laughlin [4]) and it is not reported for any of the other Cu-heavy lanthanides.

The most Gd-rich phase is GdCu. It shows congruent melting at 870°C (literature data 830°C). The structure is cubic, cP2-CsCl type and the lattice parameter is reported in Table 1.

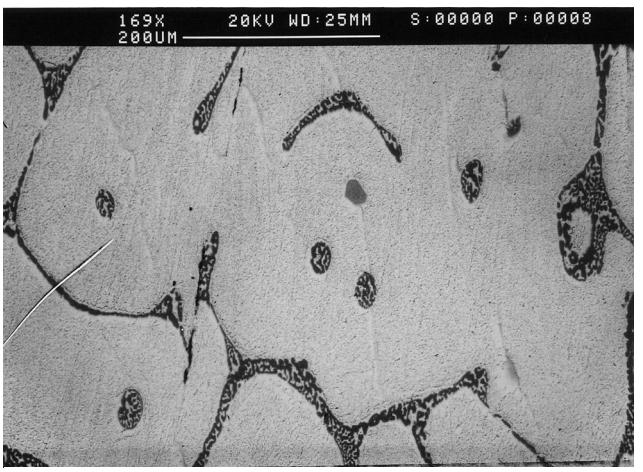

Fig. 5. BSE micrograph of Pr-4.0 at% Cu alloy, melted and cooled in DTA equipment at 5 K/min. Primary crystals of (Pr) surrounded by eutectic structure ((Pr)+PrCu). Inside the crystals small drops of catatectic liquid, showing the subsequent eutectic reaction.

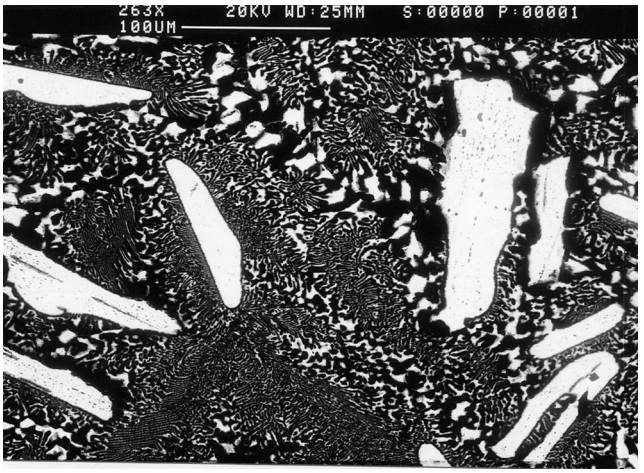

Fig. 6. BSE micrograph of Pr-25.0 at% Cu alloy, melted and cooled in DTA equipment at 5 K/min. Primary crystals of (Pr) (white) + eutectic mixture ((Pr) + PrCu).

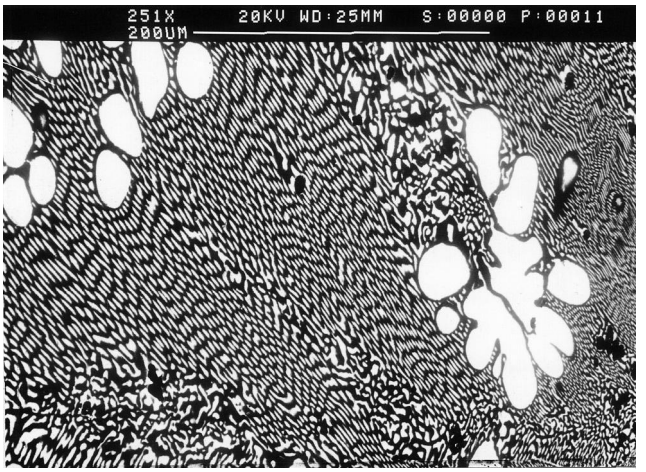

Fig. 8. BSE micrograph of Gd-30.0 at% Cu alloy, melted and cooled in DTA equipment at 5 K/min. Small amounts of (Gd) primary crystals (white) surrounded by eutectic mixture ((Gd) + GdCu).

Figs. 7 and 8 show the micrographic appearance of catatectic and eutectic alloys pertaining to the Gd-rich region of the system.

4.3. Pr–Zn system

Only five alloys have been prepared and analysed in this system at 10, 20, 30, 40 and 50 at% Zn. Differential thermal analyses, X-ray diffraction and micrographic appearance confirm the literature data from Mason and Chiotti [10], with slight differences in the temperature of the invariant equilibria. Additions of Zn to Pr lower the melting temperature of praseodymium until a eutectic reaction is reached at 570°C (literature data 576°C); also the transformation temperature of praseodymiun is lowered to a eutectoidal reaction at 550°C (literature data 558°C). The invariant reactions are:

$$L \rightleftarrows (\beta Pr) + PrZn$$

$$(\beta Pr) \rightleftarrows (\alpha Pr) + PrZn$$

Fig. 9 presents the appearance on a Pr–Zn alloy showing the above reported eutectic and eutectoidal reactions.

The most Pr-rich phase is the cubic cP2-CsCl type equiatomic phase PrZn which melts congruently at 900°C (literature data 882°C).

A few other alloys of Zn with the light rare earths, La, Ce, Nd and Sm have also been prepared in the R-rich region to better understand the effect of the additions of Zn

Fig. 7. BSE micrograph of Gd-5.0 at% Cu alloy, melted and cooled in DTA equipment at 5 K/min. Primary crystals of (Gd) surrounded by eutectic structure ((Gd) + GdCu). A typical drop of catatectic liquid, showing the subsequent eutectic reaction, can be noticed inside the central crystal.

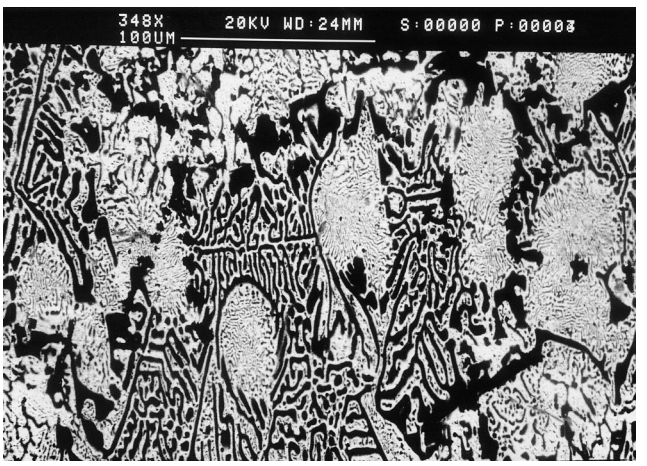

Fig. 9. BSE micrograph of Pr-20.0 at% Zn alloy, melted and cooled in DTA equipment at 5 K/min. Primary crystals of (Pr) (white) and eutectic mixture ((Pr) + PrZn). The (Pr) phase shows complete lamellar eutectoidal decomposition.

on the melting and transformation temperatures of the first rare earth metals. Alloys pertaining to the Nd–Zn and Sm–Zn system confirm the literature data from Refs. [19,20]; in both cases there is evidence of eutectoidal decomposition of the (βR). In the case of the La–Zn and Ce–Zn systems, literature data on the R-rich region are lacking. Micrographic and differential thermal analyses carried out on Ce–Zn alloys indicate the presence of a eutectic reaction at 495°C ($L \rightleftarrows (\delta Ce) + CeZn$) and of the eutectoidal decomposition of the (δCe) at 490°C ($(\delta Ce) \rightleftarrows (\gamma Ce) + CeZn$). In the case of La–Zn alloys only one invariant thermal effect was found in the La-rich region, corresponding to the La-rich eutectic at 530°C. No evidence of a eutectoidal decomposition was found; however, considering the systematic behaviour shown by the rare earth metals, a eutectoidal reaction can be expected to occur also in the La-rich end of the La–Zn system, probably at a temperature very close to that of the La-rich eutectic.

4.4. Gd–Zn system

Starting from pure gadolinium, additions of zinc lower the melting point of gadolinium from 1313°C to the Gd-rich eutectic point at 780°C and 27 at% Gd. Zinc additions also lower the $\alpha \rightleftarrows \beta$ allotropic transformation of gadolinium from 1235 to about 1200°C, giving the following catatectic reaction:

$$(\beta Gd) \rightleftarrows (\alpha Gd) + Liq$$

The type and the extent of this reaction is proposed on the basis of metallographic analyses, highlighting morphologies already described in the previously reported Cu–Pr and Cu–Gd systems. The catatectic invariant equilibria were not revealed by differential thermal analysis, even carrying out DTA runs, at variour rates, on samples with higher mass.

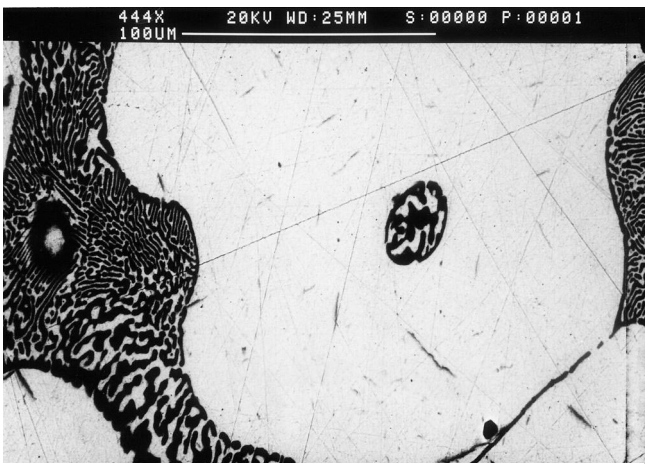

Fig. 10. BSE micrograph of Gd-8.0 at% Zn alloy, melted and cooled in DTA equipment at 5 K/min. Primary crystals of (Gd) surrounded by eutectic structure ((Gd)+GdZn). A typical drop of catatectic liquid, showing the subsequent eutectic reaction, can be noticed inside the crystal.

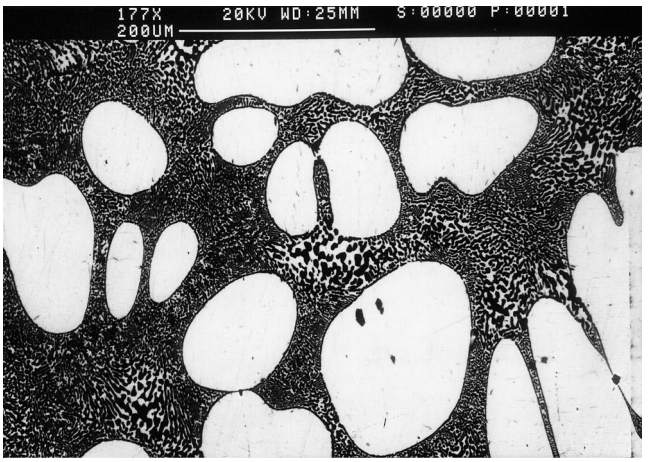

Fig. 11. BSE micrograph of Gd-15.0 at% Zn alloy, melted and cooled in DTA equipment at 5 K/min. (Gd) primary crystals (white) surrounded by eutectic mixture ((Gd)+GdZn).

Figs. 10 and 11 show the micrographic catatectic and eutectic appearances of alloys pertaining to the Gd-rich region of the system.

The estimated maximum solid solubility of Zn in βGd is about 2 at% Zn (at the invariant catatectic temperature ≈1200°C) and it is less than 1 at% Zn in αGd (at the invariant eutectic temperature, 780°C).

The most Gd-rich phase is GdZn that melts congruently at 1010°C. The crystal structure is cubic, cP2-CsCl type. The lattice parameter, obtained by the powder method and reported in Table 2, is in agreement with the literature [16].

5. Conclusions

Two types of invariant reactions have been found to occur in the Pr-rich regions of its binary systems with Cu and Zn; these are catatectic and eutectoid respectively. In the Gd-rich ends of the Gd–Cu and Gd–Zn alloy systems, only reactions of the catatectic type are found, possibly also due to the smaller difference between the melting and transformation temperatures of Gd with respect to Pr.

In the case of Pr, data relevant to the Pr-rich regions are available for several Pr–M binary systems. The effect of the 6th period elements on the melting and transformation temperatures of Pr has been studied by Griffin and Gschneidner [21]. Now, in this work, the data concerning a larger set of elements are summarized. Table 3 collects the characteristic values of the invariant equilibria of the Pr-rich ends of the binary systems formed by Pr with several elements of the 3rd, 4th, 5th and 6th periods of the Periodic Table. Fig. 12a and b report the trend of the coordinates of the Pr-rich eutectics (temperature and

Table 3
Invariant reactions occurring in the Pr-rich regions of a few binary systems of the 3rd, 4th, 5th and 6th periods of the Periodic Chart

System	Reaction	Reaction type	Composition of the phases (at% M)			Temperature °C	References
Pr–Mg	$L \rightleftarrows (\beta Pr) + PrMg$	Eutectic	40.0	≈32	≈47	735	[22]
	$(\beta Pr) \rightleftarrows (\alpha Pr) + PrMg$	Eutectoid	19.5	≈10	≈49	510	
Pr–Al	$L \rightleftarrows (\beta Pr) + \beta Pr_3Al$	Eutectic	17.5	10	25	650	[23]
	$(\beta Pr) \rightarrow (\alpha Pr) + \beta Pr_3Al$	Eutectoid	8.0	2.5	25	620	
Pr–Si	$(\beta Pr) \rightleftarrows L + (\alpha Pr)$	Catatectic	≈1	8	≈0.5	772	[24]
	$L \rightleftarrows (\alpha Pr) + \alpha Pr_5Si_3$	Eutectic	11	≈0.5	37.5	732	
Pr–Co	–	–	–			–	
	$L \rightleftarrows (Pr) + Pr_3Co$	Eutectic	19.5	0	25	570	[25]
Pr–Ni[a]	–	–	–			–	
	$L \rightleftarrows (Pr) + Pr_3Ni$	Eutectic	19	0	25	460	[26]
			20.5	0	25	540	[27]
Pr-Cu	$(\beta Pr) \rightleftarrows L + (\alpha Pr)$	Catatectic	<2	7	<1	780	This work
	$L \rightleftarrows (\alpha Pr) + PrCu$	Eutectic	30	<1	50	470	
Pr–Zn	$L \rightleftarrows (\beta Pr) + PrZn$	Eutectic	21.5	14	50	570	This work
	$(\beta Pr) \rightleftarrows (\alpha Pr) + PrZn$	Eutectoid	11	2	50	550	
Pr–Ga	$(\beta Pr) \rightleftarrows L + (\alpha Pr)$	Catatectic	6.7	10	4.2	740	[28]
	$L \rightleftarrows (\alpha Pr) + PrGa_2$	Eutectic	18.5	<0.5	33.3	580	
Pr–Ge	$(\beta Pr) \rightleftarrows L + (\alpha Pr)$	Catatectic	1.85	8.4	0	774	[29]
	$L \rightleftarrows (\alpha Pr) + Pr_3Ge$	Eutectic	12	0	25	755	
Pr–Rh	No data	–	–			–	
Pr–Pd	No data	–	–			–	
Pr–Ag	$(\beta Pr) \rightleftarrows L + (\alpha Pr)$	Catatectic	3.7	14.6	1.2	652	[30]
	$L \rightleftarrows (\alpha Pr) + AgPr$	Eutectic	22	<1	50	586	
Pr–Cd	$L \rightleftarrows (\beta Pr) + PrCd$	Eutectic	–			720	This work
	$(\beta Pr) \rightleftarrows (\alpha Pr) + PrCd$	Eutectoid	–			≈450	
Pr–In	$L \rightleftarrows (\beta Pr) + Pr_3In$	Eutectic	12	9.6	25	825	[31]
	$(\beta Pr) \rightleftarrows (\alpha Pr) + Pr_3In$	Eutectoid	8.4	5.4	25	725	
Pr–Sn	$L \rightleftarrows (\beta Pr) + Pr_3Sn$	Eutectic	10	2.9	25	794	[32]
	$(\beta Pr) \rightleftarrows (\alpha Pr) + Pr_3Sn$	Eutectoid	2.5	1.7	25	754	
Pr–Ir	$(\beta Pr) \rightleftarrows L + (\alpha Pr)$	Catatectic	0.35	8.2	<0.2	793	[21]
	$L \rightleftarrows (\alpha Pr) + Pr_5Ir_2$	Eutectic	12.1	<0.2	28.6	729	
Pr–Pt	$(\beta Pr) \rightleftarrows L + (\alpha Pr)$	Catatectic	0.45	9	<0.12	789	[21]
	$L \rightleftarrows (\alpha Pr) + Pr_7Pt_3$	Eutectic	13.4	<0.12	30	718	
Pr–Au[a]	$(\beta Pr) \rightleftarrows L + (\alpha Pr)$	Catatectic	1.56	10	<0.12	757	[21]
			2	8	<0.12	760	[33]
	$L \rightleftarrows (\alpha Pr) + Pr_2Au$	Eutectic	17.7	<0.1	33.3	619	[21]
			18	<0.1	33.3	610	[33]
Pr–Hg	$L \rightleftarrows (\beta Pr) + PrHg$	Eutectic	20.3	14.6	50	624	[21]
	$(\beta Pr) \rightleftarrows (\alpha Pr) + PrHg$	Eutectoid	12.0	0.9	50	519	
Pr–Tl	$L \rightleftarrows (\beta Pr) + Pr_3Tl$	Eutectic	13.9	9.0	25	767	[21]
	$(\beta Pr) \rightleftarrows (\alpha Pr) + Pr_3Tl$	Eutectoid	8.0	2.5	25	687	
Pr–Pb	$L \rightleftarrows (\beta Pr) + Pr_3Pb$	Eutectic	9.3	3.5	25	824	[21]
	$(\beta Pr) \rightleftarrows (\alpha Pr) + Pr_3Pb$	Eutectoid	3.1	2.2	25	778	

[a] For these systems data from different authors are given.

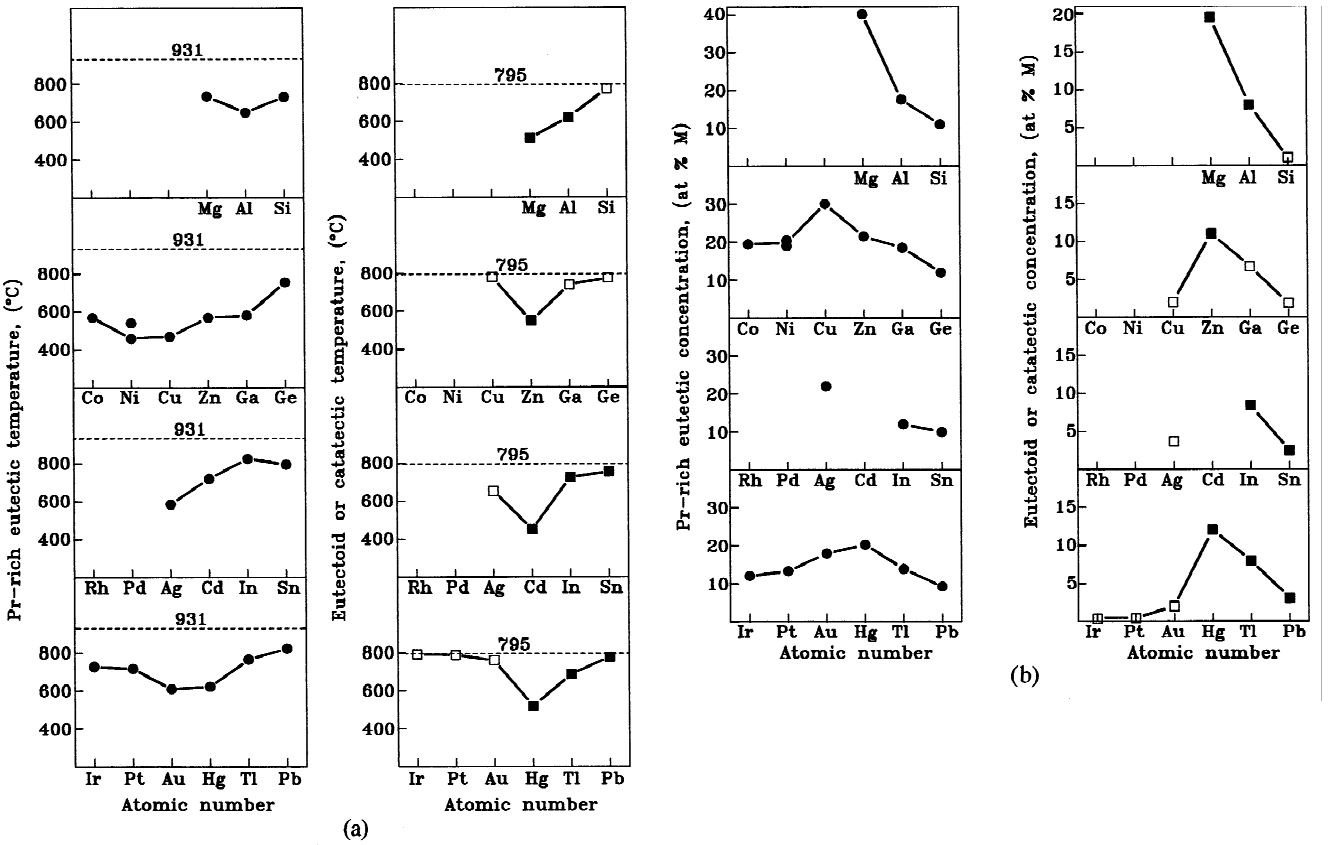

Fig. 12. Trends of the coordinates (versus the atomic number) of the invariant reactions for Pr-rich alloys of a few binary systems of the 3rd, 4th, 5th and 6th periods of the Periodic Chart. (a) Characteristic invariant temperatures. *On the left:* Temperatures of the Pr-rich eutectic (●). The 931°C melting point of Pr is reported as a reference. *On the right:* Temperature of the equilibrium (catatectic, □, or eutectoid, ■) involved in the decrease of the α to β transformation temperature of Pr by additions of a second element. The 795°C transformation temperature of Pr is reported as a reference. (b) Compositions. *On the left:* Eutectic composition of the Pr-rich eutectic (●). *O the right:* Catatectic (□) or eutectoidal (■) composition of (βPr).

concentration) and of the equilibria, catatectic and eutectoid, coming from the $\alpha \rightleftarrows \beta$ allotropic transformation of praseodymium with respect to the atomic number of the partner element.

The trends of the Pr-rich eutectic coordinates, for the elements of the 3rd (from Mg to Si), 4th and 6th periods (from Co to Ni and from Ir to Pb respectively), show a minimum of the temperature and a corresponding maximum of the concentration centred around the elements of the 11th and 12th groups (or 2nd for Mg). Similar trends (even more marked) are observed in the plots of catatectic or eutectoidal equilibria coordinates. For the elements of the 5th period (from Rh to Sn) data are scarce. They, however, seem to indicate the same trend as for the other periods, with minima of the temperature (and maxima of the concentration) around Ag and Cd. To confirm this trend, a few Pr-rich alloys of the Pr–Cd binary system have been prepared in this work and analysed by differential thermal analysis and metallography. The preliminary data so far obtained, corresponding to a eutectic halt at 720°C and a eutectoidal equilibrium at ≈450°C, have been included in Table 3 and Fig. 12a. They appear to be in agreement with the foreseen trend.

The extent of the solid solubilities of the different solutes in Pr, the trend of the mono-variant (liq/sol or α/β) equilibria and, as a consequence, the coordinates of the invariant equilibria are certainly dependent on the common metallurgical factors (size, electronegativity, etc.) which influence the alloying behaviour. The data obtained indicate, however, that, even if the solubility extent is not a simple function of one or two factors but involves the interplay of all the factors, a major role is certainly played by the group number (the valence electron number) of the solute element. We notice, indeed, a quite similar behaviour in the different periods of the Periodic Table on passing from one group to the subsequent ones.

Acknowledgements

This work is performed in the framework of the Italian ''Programmi di ricerca scientifica di rilevante interesse nazionale'' of the MURST (Ministero dell'Università e della Ricerca Scientifica e Tecnologica) and of the Italian Progetto Finalizzato ''Materiali Speciali per Tecnologie

Avanzate II'', (PF MSTA II), whose supports are acknowledged with thanks.

References

[1] T.B. Massalski, H. Okamoto, P.R. Subramanian, L. Kacprzak (Eds.), Binary Alloy Phase Diagrams, 2nd Edition, Vol. 1, ASM International, 1990.
[2] P.R. Subramanian, D.E. Laughlin, in: P.R. Subramanian, D.J. Chakrabarti, D.E. Laughlin (Eds.), Phase Diagrams of Binary Copper Alloys, ASM International, 1994.
[3] G. Canneri, Metall. Ital. 26 (1934) 869–871.
[4] P.R. Subramanian, D.E. Laughlin, Copper–Gadolinium, in: P.R. Subramanian, D.J. Chakrabarti, D.E. Laughlin (Eds.), Phase Diagrams of Binary Copper Alloys, ASM International, 1994, pp. 185–190.
[5] A.E. Dwight, Trans. ASM 53 (1961) 479–500.
[6] M. Copeland, H. Kato, in: Physics and Material Problems of Reactor Control Rods, Int. Atomic Energy Agency, Vienna, 1964, pp. 295–317.
[7] M.M. Carnasciali, S. Cirafici, E. Franceschi, J. Less-Common Metals 92 (1983) 143–147.
[8] C.S. Cheng, L.-M. Zeng, Acta Physica Sinica 32 (1983) 1443–1448.
[9] P.R. Subramanian, D.E. Laughlin, Copper–Praseodymium, in: P.R. Subramanian, D.J. Chakrabarti, D.E. Laughlin (Eds.), Phase Diagrams of Binary Copper Alloys, ASM International, 1994, pp. 322–325.
[10] J.T. Mason, P. Chiotti, Met. Trans. 1 (1970) 2119–2123.
[11] P. Villars, L.D. Calvert, H. Okamoto, Handbook of Ternary Alloy Phase Diagrams, Vols. 1–4, ASM International, Metals Park, OH, 1995.
[12] K.A. Gschneidner Jr., F.W. Calderwood, in: K.A. Gschneidner Jr., L. Eyring (Eds.), Handbook of the Physics and Chemistry of Rare Earths, Vol. 8, North-Holland Publishing, Amsterdam, 1986.
[13] R.E. Walline .W, W.E. Wallace, J. Chem. Phys. 42 (1965) 604–607.
[14] K.A. Gschneidner Jr., Acta Cryst. 18 (1965) 1082–1083.
[15] P. Morin, J. Pierre, Physica Status Solidi, Sectio A: Appl. Res. 30A (1975) 549–559.
[16] U. Köbler, W. Kinzel, W. Zinn, J. Magn. Magn. Mater. 25 (1981) 124–134.
[17] T.B. Rhinehammer, D.E. Etter, J.E. Selle, P.A. Tucker, Trans. Met. Soc. AIME 230 (1964) 1193–1198.
[18] R. Ferro, A. Saccone, S. Delfino, A.M. Cardinale, D. Macciò, Metall. Mater. Trans. B 27B (1996) 979–986.
[19] J.T. Mason, P. Chiotti, Met. Trans. 3 (1972) 2851–2855.
[20] P. Chiotti, J.T. Mason, Trans. Met. Soc. AIME 239 (1967) 547.
[21] R.B. Griffin, K.A. Gschneidner Jr., Met. Trans. 2 (1971) 2517–2524.
[22] A. Saccone, A.M. Cardinale, S. Delfino, R. Ferro, Intermetallics 1 (1993) 151–158.
[23] A. Saccone, A.M. Cardinale, S. Delfino, R. Ferro, Z. Metallkde. 87 (1996) 82–87.
[24] V.N. Eremenko, K.A. Meleshevich, Yu.I. Buyanov, Izv. V.U.Z. Tsvetn. Metall. (3) (1986) 82–87.
[25] A.E. Ray, Cobalt 1 (1974) 3–20.
[26] Y.Y. Pan, P. Nash, Nickel–Praseodymium, in: P. Nash (Ed.), Phase Diagrams of Binary Nickel Alloys, ASM, Materials Park, OH 44073, 1991, pp. 256–260.
[27] A. Saccone, A.M. Cardinale, S. Delfino, R. Ferro, Intermetallics, to be submitted.
[28] D. Dayan, G. Kimmel, J. Less-Common Metals 105 (1984) 149–160.
[29] V.N. Eremenko, Q.C. Xuong, Yu.I. Buyanov, A.M. Kharkova, Inorg. Mater. 11 (1975) 133–135.
[30] S. Delfino, A. Borsese, R. Capelli, R. Ferro, J. Less-Common Metals 35 (1974) 31–37.
[31] O.D. McMasters, K.A. Gschneidner Jr., J. Less-Common Metals 44 (1976) 281–289.
[32] V.N. Eremenko, M.V. Bulanova, V.E. Listovnichii, V.M. Petyukh, Ukr. Khim. Zh. 54 (8) (1988) 787–795.
[33] A. Saccone, D. Macciò, M. Giovannini, S. Delfino, J. Alloys and Compounds 247 (1997) 134–140.